Dynamic quantum Kerr effect in circuit quantum electrodynamics

Yi Yin,[1] H. Wang,[1,*] M. Mariantoni,[1,2] Radoslaw C. Bialczak,[1] R. Barends,[1] Y. Chen,[1] M. Lenander,[1]
Erik Lucero,[1] M. Neeley,[1,†] A. D. O'Connell,[1] D. Sank,[1] M. Weides,[1,‡] J. Wenner,[1] T. Yamamoto,[1,3]
J. Zhao,[1] A. N. Cleland,[1,2] and John M. Martinis[1,2,§]

[1]*Department of Physics, University of California, Santa Barbara, California 93106-9530, USA*
[2]*California NanoSystems Institute, University of California, Santa Barbara, California 93106-9530, USA*
[3]*Green Innovation Research Laboratories, NEC Corporation, Tsukuba, Ibaraki 305-8501, Japan*

A superconducting qubit coupled to a microwave resonator provides a controllable system that enables fundamental studies of light-matter interactions. In the dispersive regime, photons in the resonator exhibit induced frequency and phase shifts which are revealed in the resonator transmission spectrum measured with fixed qubit-resonator detuning. In this *static* detuning scheme, the phase shift is measured in the far-detuned, linear dispersion regime to avoid measurement-induced demolition of the qubit quantum state. Here we explore the qubit-resonator dispersive interaction over a much broader range of detunings, by using a *dynamic* procedure where the qubit transition is driven adiabatically. We use resonator Wigner tomography to monitor the interaction, revealing exotic nonlinear effects on different photon states, e.g., Fock states, coherent states, and Schrödinger cat states, thereby demonstrating a quantum Kerr effect in the dynamic framework.

PACS number(s): 42.50.Pq, 85.25.−j, 03.65.Wj

I. INTRODUCTION

A major focus of quantum optics is the study of atom-photon interactions at the microscopic level [1]. Atomic and solid-state cavity quantum electrodynamics (QED) systems [2–5], with strongly enhanced coupling strength between confined atoms and photons, have been developed to pursue this goal. The superconducting version, circuit QED, provides a test bed for quantum microwave photons [6] interacting with superconducting qubits [7–9]. By placing a one-dimensional transmission line resonator in close proximity to a super-conducting qubit [10–16], the electromagnetic fields in the resonator interact strongly with the qubit, forming a composite system with a modified energy spectrum [see Fig. 1(b)]. The resonator photon energy is effectively dispersed by the qubit, with a dispersion strength that depends strongly on the qubit-resonator frequency detuning. In previous experiments, the frequency and phase shift of transmitted photons were measured with a fixed qubit-resonator detuning, which we term the *static* scheme. Although the photon dispersion is well understood in this regime and provides a direct qubit readout scheme [17], it is restricted to measurements with the qubit far detuned from the resonator to avoid measurement-induced demolition of the qubit quantum state [18].

In this paper, we introduce an alternative *dynamic* scheme for measuring qubit-photon interactions. As we adiabatically change the qubit frequency, we measure the accumulated phase shift of the photons while minimizing energetic interactions with the qubit. The detuning can range from large detuning

corresponding to the linear response regime to strong nonlinear dispersion found near and at resonance. The photonic response is measured with Wigner tomography, which enables a complete map of the photon state after a dispersive interaction with the qubit [19]. We further investigate the response of completely nonclassical photon states, beyond the scope of prior static measurements, which have been restricted to measurements of classical coherent states. Measurements of the nonlinear dispersive response of superpositions of Fock states and Schrödinger cat states exhibit an excellent correspondence with the expected dynamic response and demonstrate a quantum version of the Kerr effect. Classically, the Kerr effect, a nonlinear response of macroscopic materials, is where the refractive index of a medium changes when varying the electromagnetic field strength. In this quantum version, a single qubit medium induces Fock-number-dependent phase shifts to quantum state photons. Although the near-resonant nonlinear response of coupled atom-photon systems has been previously explored using two-tone [20,21] and high-power spectroscopy [4,22–24], our approach delineates the practical aspects associated with the strong nonlinear phase shift of photons in the time domain. In the future, it should be possible to exploit the large photon phase shift resulting from small qubit-resonator detunings to improve the quantum nondemolition qubit readout with higher fidelity.

II. EXPERIMENT AND RESULTS

We use a half-wavelength superconducting coplanar waveguide (CPW) resonator coupled to a superconducting Josephson phase qubit [Fig. 1(a)]. The resonator has a fixed frequency of $\omega_r/2\pi \sim 6.32$ GHz and an energy relaxation time of $T_1 \sim 2$ μs. The flux-biased phase qubit is a strongly nonlinear electrical quantum circuit, with a tunable $|g\rangle \leftrightarrow |e\rangle$ transition angular frequency ω_q and an $|e\rangle \leftrightarrow |f\rangle$ transition frequency $\sim$200 MHz smaller ($|g\rangle$, $|e\rangle$, and $|f\rangle$ are the ground, excited, and third level qubit states) [25]. The qubit angular frequency ω_q can be tuned rapidly using quasi-dc σ_z pulses on the

*Present address: Department of Physics, Zhejiang University, Hangzhou 310027, China.

†Present address: Lincoln Laboratory, Massachusetts Institute of Technology, 244 Wood Street, Lexington, MA 02420-9108, USA.

‡Present address: National Institute of Standards and Technology, Boulder, CO 80305, USA.

§martinis@physics.ucsb.edu

inductively coupled qubit flux bias line; qubit energy level transitions are driven by π-pulse ($\sigma_{x,y}$) resonant microwave signals applied to the same line [26,27]. The qubit state can be measured destructively using a single-shot readout involving short flux pulses followed by measurement using an on-chip superconducting quantum interference device (SQUID) [28]. The qubit has a relaxation time of $T_1 \sim 450$ ns and a phase decoherence time of $T_2 \sim 150$ ns. The qubit and resonator are capacitively coupled with a coupling strength of $g/2\pi \sim 9$ MHz (i.e., the qubit-resonator gap from spectroscopy is ~ 18 MHz at resonance).

The device used in this experiment has been described in detail previously [29–31]. The fabrication process is a combination of photolithography and plasma etching on a multilayered structure, with a superconducting rhenium base film, Al/AlOx/Al Josephson junctions, and amorphous silicon for the shunt capacitor and wiring crossover dielectrics [25]. An aluminum sample box containing the wire-bonded device was mounted on the mixing chamber of a dilution refrigerator operating at $\simeq 25$ mK. The quasi-dc σ_z tuning pulse was generated by custom electronics including a field programmable gate array (FPGA)-controlled digital-to-analog (DAC) converter [25]. Two similar DAC outputs, the I and Q signals of an IQ mixer, provided the sideband mixing, phase, and pulse-shape control of the carrier signal from a microwave generator to produce the $\sigma_{x,y}$ pulse. The qubit and resonator frequencies were determined by spectroscopic measurements. The qubit-resonator coupling strength g and the resonator microwave pulse amplitude α were calibrated using a photon population analysis for a coherent state [12].

As shown for the specific case of $|0,e\rangle \leftrightarrow |1,g\rangle$ in Fig. 1(c) [where states are denoted by $|n,q\rangle$ for resonator state $|n\rangle$ and qubit state $|q\rangle$, Fig. 1(b)], the dynamic dispersion scheme involves an adiabatic procedure [32] to vary the detuning $\Delta = \omega_q - \omega_r$ and thus the eigenenergies of the qubit-resonator system. We initialize the coupled system in the far-detuned regime, where the dispersive interaction is extremely weak. We then smoothly adjust the qubit frequency as a function of time t, so that the coupled system adiabatically follows its instantaneous eigenstates with eigenenergies $E(t)$. The energy of a single photon (relative to the vacuum) is thus dispersed to $e_p(t) = E_{|1,g\rangle}(t) - E_{|0,g\rangle}(t)$, and the dynamic phase [33] accumulates as $\theta(\tau) = -\frac{1}{\hbar}\int_0^\tau [e_p(t) - e_p(0)]dt$. Although the system is returned to its initial settings at the end of the interaction, an accumulated phase shift is acquired even though the net energy exchange is zero. A Berry's phase component is ruled out because the parameter space is one dimensional. We note that the qubit-resonator coupling strength is to all practical purposes constant in our system and the detuning is time dependent, in contrast to the time-varying coupling and constant detuning displayed by Rydberg atoms passing through a microwave cavity [34–36].

We first investigated the phase shift of a one-photon Fock state due to its interaction with a qubit in its ground state. The resonator was initialized in the Fock-state superposition $|0\rangle + |1\rangle$, where $|0\rangle$ serves as a reference state [37]. The initial resonator state was prepared according to the Law-Eberly protocol, where the qubit is sequentially excited to a calculated state and partially transferred to the resonator [19]. The detuning
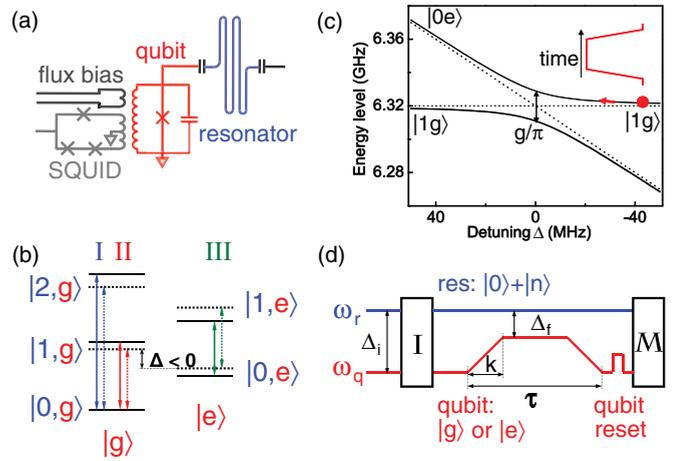

FIG. 1. (Color online) (a) Circuit diagram for the coupled qubit-resonator system. The superconducting phase qubit has a ground- to excited-state transition frequency of $\omega_q/2\pi \sim 6$ GHz. The flux bias line is coupled to the qubit through a mutual inductance. A three-junction superconducting quantum interference device (SQUID) is optimized to read out the qubit state. The CPW resonator has a constant resonant frequency of $\omega_r/2\pi \sim 6.32$ GHz. The resonator is weakly coupled to both the qubit and the external microwave source by small capacitors. (b) Energy levels of the coupled system. The solid (dashed) lines denote the energy levels with (without) the qubit-resonator interaction, with $|n,q\rangle$ representing the photon number $|n\rangle$ and the qubit state $|q\rangle$. The red (I) and blue (II) arrows represent one- and two-photon transitions with the qubit ground state. The green (III) arrows represent one-photon transitions with the qubit excited state. (c) Plot of the $|1,g\rangle$ and $|0,e\rangle$ energies as a function of detuning $\Delta = \omega_q - \omega_r$, calculated from the Jaynes-Cummings model using our experimental parameters. In an adiabatic process, the system initially at $|1,g\rangle$ [red (gray) dot] follows the path indicated by the red (gray) arrow. The resonant avoided-level crossing is $g/\pi \sim 18$ MHz. (d) Schematic of the experimental sequence, describing system initialization (labeled by "I"), adiabatically tuning and detuning the qubit, and finally performing Wigner tomography measurement (labeled by "M") of the final photon state. A reset pulse [31] to ground is applied to the qubit if it was initially prepared in the excited state, to allow the qubit to perform the measurement. The dispersive part of the pulse is also shown schematically in panel (c).

was set to $\Delta_i/2\pi = -250$ MHz, giving a small photonic component $g/\Delta_i \sim 4\%$. We then applied a trapezoidal tuning pulse to the qubit, with linear ramp rate $k = 5$ MHz/ns and interaction detuning Δ_f for an adjustable time τ [Fig. 1(d)]. At the end of the tuning pulse, the qubit was effectively decoupled from the resonator and in its ground state, with a small error due to the nonideal adiabatic process. The Wigner tomogram of the final resonator state was reconstructed by displacing the resonator state with a coherent microwave pulse (with complex amplitude α) and performing a qubit-resonator swap, from which we extracted the photon-state probability $P_n(\alpha)$ [19,38]. With sufficient sampling points α in the resonator phase space, we calculated the resonator density matrix and reconstructed the quasiprobability $W(\alpha)$ [38].

We plot the resulting Wigner functions for detuning $\Delta_f/2\pi = -57$ MHz and five different durations, τ, in the top row of Fig. 2(a). Negative quasiprobabilities are a signature
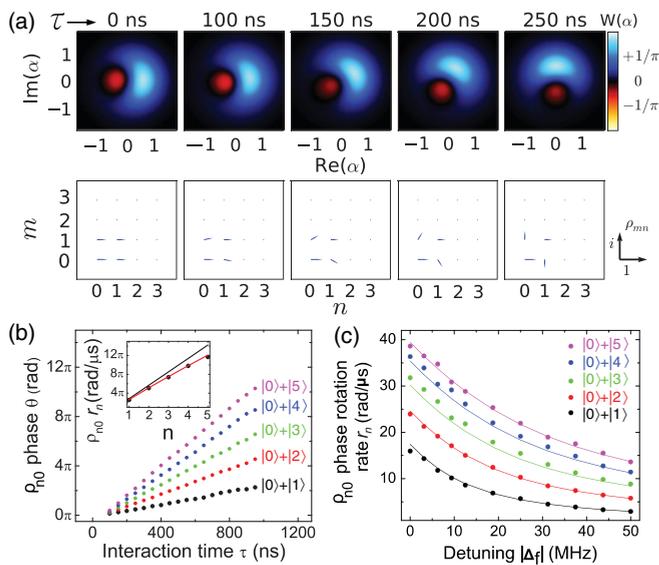
FIG. 2. (Color online) Wigner tomography and phase rotation measurement for the initial resonator state $|0\rangle + |n\rangle$. (a) Reconstructed Wigner functions for $|0\rangle + |1\rangle$ after a dispersive interaction with a ground-state qubit at $\Delta_f/2\pi = -57$ MHz for five different values of τ. The corresponding density matrices are shown in the bottom row. Sampling points [38] for $W(\alpha)$ included 60 points around two concentric circles with radii $|\alpha| = 1.10$ and 1.45. (b) Rotation angle of ρ_{n0} as a function of τ, measured from its value at $\tau = 100$ ns. (Inset) The n-dependent phase rotation rate is obtained from a linear fit to the data in panel (b). The results from both the linear approximation (black line) and the exact diagonalization [red (gray) line] of the Jaynes-Cummings Hamiltonian are displayed without any fit parameters. (c) Phase rotation speed of ρ_{n0} as a function of both Δ_f and n. Solid lines are theoretical predictions from the exact diagonalization of the Jaynes-Cummings Hamiltonian.

of the expected nonclassicality of the superposed Fock states. The diagrams are not rotationally symmetric, encoding the relative phase shift between the $|0\rangle$ and $|1\rangle$ states. As the dispersion duration τ increases, the Wigner function rotates counterclockwise about the origin. The rotation is due to an overall phase shift, induced by the qubit state during the dispersive interaction. We plot resonator density matrices in the Fock basis in the bottom row of Fig. 2(a). In each density matrix, the population probabilities ρ_{00} and ρ_{11} are nearly identical, but energy relaxation becomes more pronounced as τ increases. For $\tau = 0$ ns, the off-diagonal terms ρ_{10} and ρ_{01} are represented by horizontal arrows, indicating no phase shift as expected. As τ increases, the arrow representing ρ_{10} rotates with the same angle as that of the overall Wigner function, exhibiting an accumulated nonzero phase shift; the time dependence of this phase rotation angle is shown in Fig. 2(b). The constant rotation rate represents a phase rotation speed of $r_0 = d\theta/d\tau = 3.1\pi$ rad/μs and is equal to the expected frequency shift of the one-photon state $|1\rangle$ at the detuning Δ_f.

We next investigated higher-number photon states by initializing the resonator in $|0\rangle + |n\rangle$ with n from 2 to 5. Following the same pulse sequence, the density matrices and the Wigner functions of the final photon states were measured. Figure 2(b) shows the phase rotation angles of

the ρ_{n0} element of the density matrix versus τ. Linear fits allow us to extract the n-dependent phase rotation speed. In the far-detuned regime, the angular frequency shift scales as expected with photon number as $ng^2/|\Delta_f|$ [cf. Eq. (3) in the Appendix]. This linear approximation [black line, Fig. 2(b) inset] deviates from experimental data as n increases, because the dressed photon energies become anharmonic; a rigorous solution of the Jaynes-Cummings model [cf. Eq. (1) in the Appendix] is in good agreement with the data [red (gray) line, Fig. 2(b) inset]. The phase rotation rate as a function of detuning Δ_f [Fig. 2(c)] is also in excellent agreement with the full Jaynes-Cummings model, extending the nonlinear response measurements to zero detuning. This rate corresponds to the refractive index of macroscopic materials, where a single qubit, as an effective electric dipole, is the index medium which interacts with the electric field of quantum state photons. The Fock-state-dependent phase shifts imply a photon-number-dependent change in the refractive index of the medium, demonstrating a quantum Kerr effect in the dynamic framework. Although the energy levels of the qubit-resonator system can be measured using spectroscopy [39], here the nonlinear phase shift in the strong dispersive regime is directly and quantitatively measured in the time domain in a circuit QED system.

In a standard resonator transmission measurement, a coherent state $|\alpha\rangle$ is injected in the resonator by a classical microwave pulse. Here we prepared a coherent resonator photon state with complex amplitude $\alpha \sim 2.0$ and applied the dynamic scheme to measure the phase shift induced by interaction with a ground-state qubit. Figure 3(a) presents the measurement after a trapezoid pulse at $\Delta_f/2\pi = -50$ MHz. The Wigner function of the initial state ($\tau = 0$ ns) shows a coherent peak centered at α and a symmetric noise of quantum uncertainty. As τ increases, the coherent peak rotates counterclockwise about the origin, with only a slight and gradual increase in distortion. For each Fock constituent, the linear approximation gives a phase shift rate of $r_n \sim nr_0 = ng^2/|\Delta_f|$. The coherent state is thus uniformly transformed to $|\alpha e^{ir_0\tau}\rangle$ after time τ, based on the Poissonian distribution. In the Wigner representation, each Fock constituent has a rotation rate of $r_{w,n} = r_n/n = r_0$ and the Wigner function rotates as a whole with the rotation angle $r_0\tau$, which is equal to the phase shift measured in a resonator transmission measurement. This simple behavior is most accurate in the far-detuned regime, where the dressed resonator levels are still nearly equally spaced. At small detuning, where anharmonicity becomes more significant, the various Fock components begin to rotate out of phase and the Wigner function begins to display squeezing [see Fig. 3(a)].

To further illustrate the linear-nonlinear crossover of the dispersive interaction, we investigated the Schrödinger cat state $|\alpha = \sqrt{2}i\rangle + |\alpha = -\sqrt{2}i\rangle$. In Fig. 3(b) we display the reconstructed Wigner functions for four different values of detuning Δ_f and three interaction times τ. At zero interaction time, the Wigner function contains two well-separated Gaussian peaks, arising from the two coherent state elements, with clear interference fringes between the two peaks. The Wigner function rotates counterclockwise with increasing time τ, as before. For detuning $\Delta_f/2\pi = -56$ MHz, the shape
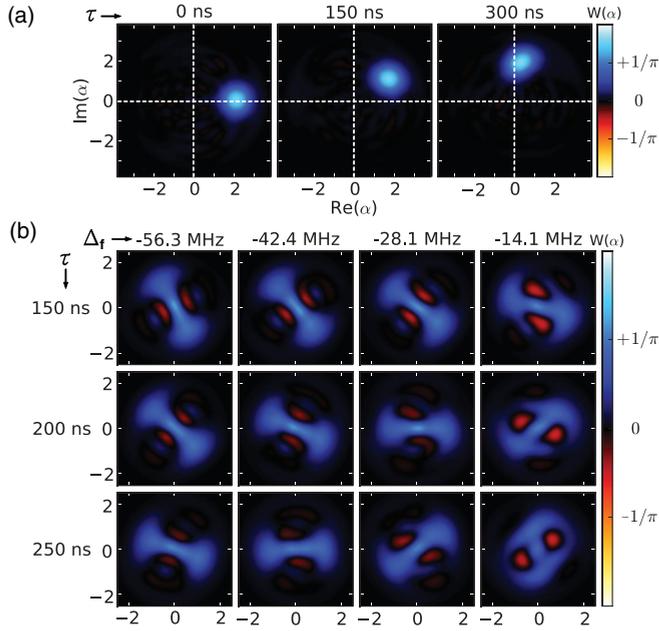
FIG. 3. (Color online) (a) Wigner functions and density matrices for a coherent state ($\alpha \sim 2.0$) interacting with a ground-state qubit at three different durations τ for detuning $\Delta_f/2\pi = -50$ MHz. Axes at the origin are indicated. The center of the coherent-state Wigner function rotates counterclockwise about the origin with time. (b) Wigner functions for a Schrödinger cat state $|\alpha = \sqrt{2}i\rangle + |\alpha = -\sqrt{2}i\rangle$ after different interaction times with a ground-state qubit. A fixed detuning Δ_f from -56.3 to -14.1 MHz was used for each column. As the duration τ increases from 150 to 250 ns, the Wigner function rotates counterclockwise, with the rotation rate increasing as the absolute value of detuning Δ_f decreases. For small detunings, enhanced distortions appear in both the coherent peaks and the interference fringes.

of the Wigner function is almost preserved as τ increases, consistent with expectations from the linear approximation. As the absolute value of detuning Δ_f decreases, the rotation speed increases and distortion becomes significant. The two Gaussian peaks are twisted and the interference fringes deform with time, due to the differing rotation speeds of the Fock components. This strongly nonlinear effect is most prominent for zero detuning, where the rotation rate scales as $r_{w,n} \propto 1/\sqrt{n}$ [20,23].

The examples above were measured with a qubit initialized in its ground state, for which qubit relaxation and phase decoherence are less important. We also examined the response of a resonator interacting with a qubit initialized in the excited state. Figure 4(a) shows the Wigner function for a resonator initialized in $|0\rangle + |1\rangle$ after interacting with an excited-state qubit at detuning $\Delta_f/2\pi = -35$ MHz. In contrast to the response seen with a ground-state qubit, we observe the opposite rotation direction, indicating a negative shift in photon frequency and phase. The nonclassical negative quasiprobabilities of the Wigner function diminish much more quickly, in accordance with the rapid decoherence of the off-diagonal terms in the density matrix. In addition, for three different final detunings Δ_f [Fig. 4(b)], the phase rotation angle of ρ_{01} is no longer linearly dependent on τ but
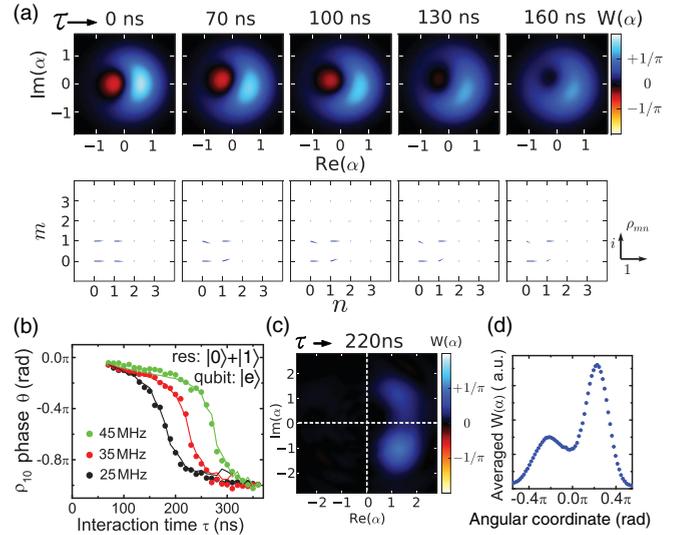

FIG. 4. (Color online) Measurement of photon states after dispersive interaction with an excited-state qubit. To minimize qubit relaxation during the interaction, we use a higher tuning ramp speed of $k = 7$ MHz/ns. The qubit was reset to its ground state prior to the tomography measurement by transferring the excitation to a nearby two-level state using an iSWAP gate [31]. (a) Wigner functions and density matrices for the initial resonator state $|0\rangle + |1\rangle$. The dispersive interaction was measured for detuning $\Delta_f/2\pi = -35$ MHz for five different durations τ. (b) Rotation angle for ρ_{10} vs τ for three different detunings Δ_f. Solid lines are numerical simulations of the Lindblad master equation including both system decoherence and the third level of the qubit. However, we have to use a shorter qubit decoherence time to yield reasonable agreement between the experimental and theoretical results. For $|\Delta_f|/2\pi$ of 25, 35, and 45 MHz, the qubit relaxation times T_1 were 200, 220, and 250 ns, respectively. (c) Wigner function for a coherent state after interacting with an excited-state qubit for $\tau = 220$ ns at $\Delta_f/2\pi = -75$ MHz. (d) Radially averaged $W(\alpha)$ as a function of the angular coordinate, extracted from the Wigner function in panel (c).

shows a periodic S-shaped structure [Fig. 4(b)], which can be related to qubit relaxation.

To understand the effects of qubit relaxation, we investigated the response of a coherent photon state [Fig. 4(c)]. During the dispersive interaction, the qubit can relax at any moment, performing a stochastic quantum jump in its time trajectory. As a consequence, the coherent peak in the Wigner function will initially rotate clockwise, but when the qubit relaxes it will switch to a counterclockwise rotation for the remainder of the dispersive interaction. The amplitude of the jump probability is determined by the qubit relaxation time T_1 and decays exponentially as time increases. The reconstructed Wigner function thus comprises the main coherent peak (from the excited-state qubit) accompanied by a small peak with a tail (due to rotation from the ground-state qubit). Numerical simulations of the Lindblad master equation are quantitatively consistent with the experimental results (not shown).

For a general resonator state interacting with an excited qubit, the qubit relaxation and the mixed qubit state lead to a decoherence effect on the final photon state. The decoherence effect is averaged over many individual quantum jumps in the ensemble measurement required for collecting quantum

statistics. For a resonator initialized in $|0\rangle + |1\rangle$, the excited qubit disperses the photons with a phase shift, i.e., rotates the horizontal off-diagonal vector ρ_{01} to an angle $\theta(\tau)$. The off-diagonal terms from qubit quantum jumps are represented by vectors with rotation angles distributed over the range $[\theta(\tau), -\theta(\tau)]$ and amplitudes corresponding to the probability of the specific quantum jump. Averaging over all the vectors resulting from quantum jumps decreases the phase rotation angle of ρ_{01} when θ is small, i.e., still an acute angle. When θ is larger than $\pi/2$, the averaged vectors from the qubit relaxation increase the phase rotation angle. This explains the S-shaped structure in the time-dependent phase rotation angles [Fig. 4(b)]. These data are in fact predicted [Fig. 4(b)] from numerical simulations using the Lindbald master equation (cf. the Appendix) incorporating the third qubit level, qubit decoherence, and two-level states (TLS).

III. CONCLUSIONS

In conclusion, we have used an adiabatic dynamic control of the qubit to study its dispersive interaction with a cavity resonator. In this dynamic scheme, the frequency shift of multiphoton Fock states is extended to the strongly nonlinear dispersive regime, close to zero detuning. We can fully control and measure the accumulated phase shift of complex photon states, demonstrated by the excellent agreement between the experimental data and the theoretical prediction. In the strongly nonlinear dispersive regime, a quantum Kerr effect is observed for the coherent and other nonclassical photon states: We illustrate the nonlinear response of photons to the refractive index effect of our artificial atom using Wigner tomography. Furthermore, we reveal the distinct phase shift of photons induced by the excited-state qubit, and we interpret the peculiar photon decoherence resulting from qubit-state relaxation.

APPENDIX: MODELING AND SIMULATION

The coupled qubit-resonator system is described by the Jaynes-Cummings Hamiltonian [1], $H = \hbar\omega_r(a^\dagger a + 1/2) + \hbar\omega_q\sigma_z/2 + \hbar g(\sigma^+ a + a^\dagger\sigma^-)$, where $\hbar\omega_r$ is the single photon energy of the relevant electromagnetic field mode, $\hbar\omega_q$ is the excitation energy of the qubit, and $a^\dagger(a)$ and $\sigma^+(\sigma^-)$ are the creation (destruction) operators for the resonator photons

and the qubit, respectively. With the coupling strength g, the interaction term describes the energy exchange between the qubit and the resonator. The photon energy is effectively dispersed by virtual energy exchange when an electromagnetic wave transmits through the resonator at a detuning of $\Delta = \omega_q - \omega_r$. In the Jaynes-Cummings model, the qubit-resonator interaction leads to two eigenenergies, $n\hbar\omega_r \pm \frac{\hbar}{2}\sqrt{4g^2n + \Delta^2}$, for each state pair $|n,g\rangle$ and $|n-1,e\rangle$ ($\Delta < 0$ is assumed). As shown in Fig. 1(b), the energy of an n-photon state is dispersed to

$$ne_{p,g} = E_{|n,g\rangle} - E_{|0,g\rangle}$$
$$= n\hbar\omega_r + \frac{\hbar}{2}\left(\sqrt{4g^2n + \Delta^2} - |\Delta|\right), \qquad \text{(A1)}$$

when interacting with a ground-state qubit. With the excited-state qubit, the dispersed energy becomes

$$ne_{p,e} = E_{|n,e\rangle} - E_{|0,e\rangle}$$
$$= n\hbar\omega_r - \frac{\hbar}{2}\left(\sqrt{4g^2(n+1) + \Delta^2} - \sqrt{4g^2 + \Delta^2}\right). \qquad \text{(A2)}$$

In the far-detuned regime, the linear approximation is applied and the n-photon energy is simplified to be

$$ne_{p,\sigma_z} \simeq n\hbar\omega_r + \sigma_z n\hbar g^2/\Delta \qquad \text{(A3)}$$

for the ground-state and excited-state qubit (represented by σ_z).

The dispersive qubit-resonator interaction can be strongly affected by the qubit relaxation and decoherence. Our numerical simulations used the Markovian Lindblad master equation for the system density matrix ρ,

$$\frac{d\rho}{dt} = -\frac{i}{\hbar}[H(t),\rho] + \sum_{L_1,L_2} L \cdot \rho \cdot L^\dagger - \frac{1}{2}L^\dagger \cdot L \cdot \rho$$
$$- \frac{1}{2}\rho \cdot L^\dagger \cdot L,$$

where $H(t)$ is the instantaneous total Hamiltonian and two superoperators, $L_1 = 1/\sqrt{T_1}\sigma^-$ and $L_2 = 1/\sqrt{T_2}\sigma^+\sigma^-$, describe qubit relaxation and decoherence. To simulate the phase qubit, the third qubit level can be added in the numerical master equation. We find that for the photon-state phase shift induced by a ground-state qubit, the numerical results of the master equation including decoherence and the third level contribution are very close to the analytic solution of the Jaynes-Cummings Hamiltonian without dissipation, with differences smaller than our experimental resolution. For photons interacting with an excited qubit, in contrast, numerical simulations with both decoherence and the third level have to be applied when comparing experimental data with theoretical results [see Fig. 4(b)].

[1] D. E. Walls and G. J. Milburn, *Quantum Optics* (Spring-Verlag, Berlin, 1994).

[2] H. Mabuchi and A. C. Doherty, Science **298**, 1372 (2002).

[3] S. Haroche and J.-M. Raimond, *Exploring the Quantum—Atoms, Cavities and Photons* (Oxford University Press, Oxford, UK, 2006).

[4] I. Schuster, A. Kubanek, A. Fuhrmanek, T. Puppe, P. W. H. Pinkse, K. Murr, and G. Rempe, Nat. Phys. **4**, 382 (2008).

[5] K. Hennessy, A. Badolato, M. Winger, D. Gerace, M. Atatüre, S. Gulde, S. Fält, E. L. Hu, and A. Imamoğlu, Nature (London) **445**, 896 (2007).

[6] R. J. Schoelkopf and S. M. Girvin, Nature (London) **451**, 664 (2008).

[7] John Clarke and Frank K. Wilhelm, Nature (London) **453**, 1031 (2008).

[8] Y. Makhlin, G. Schon, and A. Shnirman, Rev. Mod. Phys. **73**, 357 (2001).

[9] J. Q. You and Franco Nori, Phys. Today **58**(11), 42 (2005).

[10] A. Wallraff, D. I. Schuster, A. Blais, L. Frunzio, R.-S. Huang, J. Majer, S. Kumar, S. M. Girvin, and R. J. Schoelkopf, Nature (London) **431**, 162 (2004).

[11] I. Chiorescu, P. Bertet, K. Semba, Y. Nakamura, C. J. P. M. Harmans, and J. E. Mooij, Nature (London) **431**, 159 (2004).

[12] Max Hofheinz, E. M. Weig, M. Ansmann, Radoslaw C. Bialczak, Erik Lucero, M. Neeley, A. D. O'Connell, H. Wang, John M. Martinis, and A. N. Cleland, Nature (London) **454**, 310 (2008).

[13] O. Astafiev, K. Inomata, A. O. Niskanen, T. Yamamoto, Yu. A. Pashkin, Y. Nakamura, and J. S. Tsai, Nature (London) **449**, 588 (2007).

[14] Mika A. Sillanpää, Jae I. Park, and Raymond W. Simmonds, Nature (London) **449**, 438 (2007).

[15] R. H. Koch, G. A. Keefe, F. P. Milliken, J. R. Rozen, C. C. Tsuei, J. R. Kirtley, and D. P. DiVincenzo, Phys. Rev. Lett. **96**, 127001 (2006).

[16] J. Johansson, S. Saito, T. Meno, H. Nakano, M. Ueda, K. Semba, and H. Takayanagi, Phys. Rev. Lett. **96**, 127006 (2006).

[17] A. Wallraff, D. I. Schuster, A. Blais, L. Frunzio, J. Majer, M. H. Devoret, S. M. Girvin, and R. J. Schoelkopf, Phys. Rev. Lett. **95**, 060501 (2005).

[18] D. I. Schuster, A. A. Houck, J. A. Schreier, A. Wallraff, J. M. Gambetta, A. Blais, L. Frunzio, J. Majer, B. Johnson, M. H. Devoret, S. M. Girvin, and R. J. Schoelkopf, Nature (London) **445**, 515 (2007).

[19] Max Hofheinz, H. Wang, M. Ansmann, Radoslaw C. Bialczak, Erik Lucero, M. Neeley, A. D. O'Connell, D. Sank, J. Wenner, John M. Martinis, and A. N. Cleland, Nature (London) **459**, 546 (2009).

[20] J. M. Fink, M. Göppl, M. Baur, R. Bianchetti, P. J. Leek, A. Blais, and A. Wallraff, Nature (London) **454**, 315 (2008).

[21] Frank Deppe, Matteo Mariantoni, E. P. Menzel, A. Marx, S. Saito, K. Kakuyanagi, H. Tanaka, T. Meno, K. Semba, H. Takayanagi, E. Solano, and R. Gross, Nat. Phys. **4**, 686 (2008).

[22] M. Brune, F. Schmidt-Kaler, A. Maali, J. Dreyer, E. Hagley, J. M. Raimond, and S. Haroche, Phys. Rev. Lett. **76**, 1800 (1996).

[23] Lev S. Bishop, J. M. Chow, Jens Koch, A. A. Houck, M. H. Devoret, E. Thuneberg, S. M. Girvin, and R. J. Schoelkopf, Nat. Phys. **5**, 105 (2009).

[24] M. D. Reed, L. DiCarlo, B. R. Johnson, L. Sun, D. I. Schuster, L. Frunzio, and R. J. Schoelkopf, Phys. Rev. Lett. **105**, 173601 (2010).

[25] John M. Martinis, Quantum Inf. Process. **8**, 81 (2009).

[26] Erik Lucero, M. Hofheinz, M. Ansmann, Radoslaw C. Bialczak, N. Katz, Matthew Neeley, A. D. O'Connell, H. Wang, A. N. Cleland, and John M. Martinis, Phys. Rev. Lett. **100**, 247001 (2008).

[27] Erik Lucero, Julian Kelly, Radoslaw C. Bialczak, Mike Lenander, Matteo Mariantoni, Matthew Neeley, A. D. O'Connell, Daniel Sank, H. Wang, Martin Weides, James Wenner, Tsuyoshi Yamamoto, A. N. Cleland, and John M. Martinis, Phys. Rev. A **82**, 042339 (2010).

[28] Matthew Neeley, M. Ansmann, Radoslaw C. Bialczak, M. Hofheinz, N. Katz, Erik Lucero, A. O'Connell, H. Wang, A. N. Cleland, and John M. Martinis, Phys. Rev. B **77**, 180508 (2008)

[29] Matteo Mariantoni, H. Wang, Radoslaw C. Bialczak, M. Lenander, Erik Lucero, M. Neeley, A. D. O'Connell, D. Sank, M. Weides, J. Wenner, T. Yamamoto, Y. Yin, J. Zhao, John M. Martinis, and A. N. Cleland, Nat. Phys. **7**, 287 (2011).

[30] H. Wang, M. Mariantoni, Radoslaw C. Bialczak, M. Lenander, Erik Lucero, M. Neeley, A. D. O'Connell, D. Sank, M. Weides, J. Wenner, T. Yamamoto, Y. Yin, J. Zhao, John M. Martinis, and A. N. Cleland, Phys. Rev. Lett. **106**, 060401 (2011).

[31] Matteo Mariantoni, H. Wang, T. Yamamoto, M. Neeley, Radoslaw C. Bialczak, Y. Chen, M. Lenander, Erik Lucero, A. D. O'Connell, D. Sank, M. Weides, J. Wenner, Y. Yin, J. Zhao, A. N. Korotkov, A. N. Cleland, and John M. Martinis, Science **334**, 61 (2011).

[32] B. R. Johnson, M. D. Reed, A. A. Houck, D. I. Schuster, Lev S. Bishop, E. Ginossar, J. M. Gambetta, L. DiCarlo, L. Frunzio, S. M. Girvin, and R. J. Schoelkopf, Nat. Phys. **6**, 663 (2010).

[33] M. V. Berry, Proc. R. Soc. London A **392**, 45 (1984).

[34] M. Brune, P. Nussenzveig, F. Schmidt-Kaler, F. Bernardot, A. Maali, J. M. Raimond, and S. Haroche, Phys. Rev. Lett. **72**, 3339 (1994).

[35] Sébastien Gleyzes, S. Kuhr, C. Guerlin, J. Bernu, S. Deléglise, Ulrich Busk Hoff, M. Brune, Jean-Michel Raimond, and S. Haroche, Nature (London) **446**, 297 (2007).

[36] Christine Guerlin, J. Bernu, S. Deléglise, C. Sayrin, S. Gleyzes, S. Kuhr, M. Brune, Jean-Michel Raimond, and S. Haroche, Nature (London) **448**, 889 (2007).

[37] Matthew Neeley, M. Ansmann, Radoslaw C. Bialczak, M. Hofheinz, Erik Lucero, A. O'Connell, Daniel Sank, H. Wang, J. Wenner, A. N. Cleland, M. R. Geller, and John M. Martinis, Science **325**, 722 (2009).

[38] H. Wang, M. Hofheinz, M. Ansmann, R. C. Bialczak, Erik Lucero, M. Neeley, A. D. O'Connell, D. Sank, M. Weides, J. Wenner, A. N. Cleland, and John M. Martinis, Phys. Rev. Lett. **103**, 200404 (2009).

[39] A. Fragner, M. Göeppl, J. M. Fink, M. Baur, R. Bianchetti, P. J. Leek, A. Blais, and A. Wallraff, Science **322**, 1357 (2008).